ELSEVIER

Contents lists available at ScienceDirect

# **Chemical Physics Impact**

journal homepage: www.sciencedirect.com/journal/chemical-physics-impact



Full Length Article

# Influence of PVP on the properties of solvothermally synthesized famatinite nanoparticles: Structural, morphological and optical insights

Prakash Iruthayanathan <sup>a</sup>, Anne Sarah Christinal <sup>a</sup>, Amutha Soosairaj <sup>a</sup>, Leo Rajesh Asirvatham <sup>b,\*</sup>

#### ARTICLE INFO

#### Keywords: Famatinite Solvothermal Binary solvent Polyvinylpyrrolidone Tetragonal crystal structure

#### ABSTRACT

Famatinite ( $Cu_3SbS_4$ ) nanoparticles were synthesized through a solvothermal approach using various polyvinylpyrrolidone (PVP) ratios as a capping agent with a binary solvent of ethylene glycol and water in equal parts. Incremental additions of PVP, ranging from 0 to 1.5 g, exerted significant influence on the material's characteristics. Through comprehensive analysis involving X-ray diffraction, Raman spectroscopy, Scanning electron microscopy (SEM) with Energy dispersive spectrometer (EDS), and UV diffuse reflectance spectroscopy, critical insights were obtained. XRD analysis confirmed the tetragonal crystal structure and revealed reduced crystallite sizes due to the incorporation of PVP. Raman spectroscopy validated the presence of pure famatinite phase with 0.5 g and 1.0 g PVP. SEM analysis uniformly depicted a spherical morphology in all samples, emphasizing PVP's role in mitigating nanoparticle agglomeration. UV diffuse reflectance spectroscopy disclosed direct bandgaps falling within the 0.88 – 0.97 eV range. The collective findings highlighted the substantial impact of PVP in the binary solvent on the structural, morphological, and optical properties of  $Cu_3SbS_4$  nanoparticles. These results underscore the potential application of these tailored nanoparticles as promising candidates for advanced photovoltaic absorber materials.

# 1. Introduction

In the quest for more efficient, versatile, and cost-effective solar energy, thin-film photovoltaics have emerged as a prime example. Thin-film photovoltaics represent a transformative leap in solar energy technology, offering a lightweight, flexible, abundant and cost-effective alternative to traditional silicon-based cells [1–3]. Cu-Sb-S based materials are still in the early phases of study, but their non-toxic composition and tunable features make them a possible sustainable substitute for hazardous absorber materials based on Cd, Te, Pb, and Se as well as for the scarce In and Ga based absorber materials [4]. The challenge lies in optimizing their performance to match or surpass the efficiency levels of CdTe (20.6 %), CIGS (20.8 %) [5], DSSC (13 %) [6], CZTS (11 %) [7] and perovskite (15.4 %) [8] based photovoltaic materials.

Tenary copper antimony sulphide compound has four phases:  $CuSbS_2$  (Chalcostibite) [8,9,10],  $Cu_3SbS_4$  (Famatinite) [11,12],  $Cu_3SbS_3$  (Skinnerite) [13], and  $Cu_{12}Sb_4S_{13}$  (Tetrahedrite) [14,15]. Their diverse range of optical and electrical properties, high absorption coefficient of

around 10<sup>5</sup> cm<sup>-1</sup> and p-type conductivity make them ideal candidates for use as p-type absorber materials in photovoltaics. These phases offer a spectrum of bandgap values, typically ranging from around 0.5-2 eV, making them well-suited for absorbing a broad range of solar spectrum [16]. Scientists and engineers can experiment with these materials' tunable qualities to optimise the efficiency of solar cells. Tailoring the bandgap and optimizing the electronic structure could lead to enhanced efficiency and stability, making Cu-Sb-S group materials stand out in the crowded field of photovoltaics [17]. Famatinite (Cu<sub>3</sub>SbS<sub>4</sub>) has been gaining attention as a promising absorber layer in solar cells since it exhibits excellent light absorption characteristics, especially in the visible and near-infrared regions of the solar spectrum [18]. Famatinite nanoparticles can be synthesized over a variety of methods [19-22], and these methods typically involve mixing precursor solutions or reactants under controlled conditions, enabling the gradual formation and growth of nanoparticles with desired properties. The adjustment of parameters such as temperature, pressure, precursor concentrations, and reaction times allows precise control over the synthesis process, providing

E-mail address: aleorajesh@gmail.com (L.R. Asirvatham).

a Department of Physics, St. Joseph's College (Autonomous), Affiliated to Bharathidasan University, Tiruchirappalli 620002, India

b Department of Physics, School of Physical, Chemical and Applied Sciences, Pondicherry University, Puducherry 605014, India

 $<sup>^{\</sup>ast}$  Corresponding author.

opportunities for customized applications in fields like solar energy, thermoelectric energy [23] and optoelectronics [24].

Changhua An et al. used a mild hydrothermal process to synthesize Cu<sub>3</sub>SbS<sub>4</sub> nanofibers, and the reaction temperature and medium greatly influenced the phases and the morphology of the final product [21]. Qun Wang et al. produced hierarchical flower-like microspheres composed of Cu<sub>3</sub>SbS<sub>4</sub> nanoflakes doped with chlorine (Cl-) through a one-pot solvothermal ion exchange process. This synthesis method utilized a solvent mixture consisting of 3:1 ethylene glycol to acetylacetone. [25]. M. Bella et al. synthesised pure Cu<sub>3</sub>SbS<sub>4</sub> nanocrystals by varying the surfactant to solvent volumetric ratio and sulfer to copper molar ratio [11]. Sulawan Kaowphong et al. prepared CuInS2 nanoparticles by using a mixed solvent of water and ethylene glycol (1:1) as a liquid medium, expecting that altering the reaction medium could tailer the characteristics of the synthesized CuInS<sub>2</sub> particles, such as purity, crystallinity, shape, particle size, and particle size distribution [22]. In order to prevent the formation of a well-crystalline metal ion-En complex, Mou Pal et al. reported the synthesis of phase pure chalcostibite CuSbS2 nanocrystals by employing ethylenediamine and deionized water with varied ratios as solvent by solvothermal technique [26].

Polymers have been widely used in various applications due to outstanding properties such as their low cost, stability, easy fabrication, etc. [27]. Furthermore, their favorable mechanical, thermal, and electrical characteristics have rendered them highly intriguing for both research and industrial applications [28]. Polymer blends have recently emerged as highly promising materials for many applications including solar cells, sensors, energy storage, as well as water desalination [29]. One such polymer is PVP, which has been found to exhibit chemical inertness, non-toxic, and readily soluble in water [30]. PVP is a significant polymer due to its capacity to improve physical qualities [31]. In their solvothermal synthesis of Cu-Sb-S nanoparticles, Bincy John et al. utilized PVP as a size-reducing agent and to stabilize the growth and formation of well-defined structure [32]. In their recent study Kallum et al. reported that PVP can serves as an excellent stabilizer and shape-directing agent in the synthesis of metal chalcogenide (MC) nanoparticles, preventing their aggregation and passivating surface states. They also noted that the utilization of PVP can improve optical properties under specific circumstances [33].

B. John et al. reported on the effects of PVP on the structural, morphological, optical, and electrical properties of the synthesised  $\text{CuSbS}_2$  nanoparticles by the solvothermal method using ethylene glycol as solvent [34]. The influence of varying PVP ratios on the phase composition and morphology of  $\text{CuSbS}_2$  nanoparticles that were synthesised by microwave radiation was investigated by Wei Wang et al. [35]. The above-mentioned research articles employed varied solvent compositions and adjusted capping agent concentrations. This deliberate manipulation enables us to customize the chemical and physical properties of  $\text{Cu}_3\text{SbS}_4$  nanoparticles within the solvothermal system.

The present research utilized a novel mixed binary solvent composed of distilled water and ethylene glycol to initiate the synthesis of tetragonal famatinite nanocrystals. The quantity of the capping agent (polyvinylpyrrolidone, PVP) was varied to modify the structural, morphological, and optical characteristics of the material. During the synthesis process, PVP is essential for stabilising nanoparticles and regulating their growth by preventing them from agglomerating or getting too big. The size, shape, crystal structure and morphology of the synthesized Cu<sub>3</sub>SbS<sub>4</sub> nanoparticles were influenced by the concentration of PVP used. The findings of this work will make a captivating subject in the ongoing quest for more efficient, earth abundant, less toxic, affordable and promising photovoltaic absorber material.

# 2. Experimental procedure

#### 2.1. Chemicals

Copper (II) chloride dihydrate (CuCl<sub>2</sub>·2H<sub>2</sub>O) and antimony

trichloride (SbCl $_3$ ) were purchased from Sigma Aldrich. Thiourea (CH $_4$ N $_2$ S) was purchased from Loba Chemie Pvt. Ltd. Polyvinylpyrrolidone (PVP) with a molecular weight of 40000 was purchased from Sisco Research Laboratories Pvt. Ltd (SRL). Ethylene glycol was purchased from Merck. All the chemicals purchased were in analytical grade and used without further purification.

#### 2.2. Synthesis of Cu<sub>3</sub>SbS<sub>4</sub> nanoparticles

The synthesis of famatinite nanoparticles employed a simple solvothermal approach utilizing a binary solvent. This solvent was prepared by mixing 75 ml of ethylene glycol with 75 ml of distilled water, resulting in a total volume of 150 ml. To this solvent mixture, 25 mM of copper (II) chloride dihydrate, 25 mM of antimony trichloride, and 75 mM of thiourea were added and stirred for 30 min. This solution was labelled as PVP<sub>0</sub> because polyvinylpyrrolidone (PVP) was not added during the synthesis process. Subsequent solutions, designated as  $PVP_{0.5}$ ,  $PVP_{1.0}$ , and  $PVP_{1.5}$ , were prepared by adding varying amounts of PVP (0.5 g, 1.0 g, and 1.5 g, respectively) during the stirring process. Following preparation, each solution was transferred straight into a 200 ml teflon-lined autoclave and subjected to a temperature of 180°C for 24 h in a hot air oven. Once the desired time elapsed, the hot air oven was allowed to cool down to room temperature. Then, the autoclave was removed from the oven, and the resulting nanoparticles were recovered by repeated centrifugation using distilled water and ethanol at 3000 rpm for 10 min, aiming to remove excess capping agent, reaction byproducts, and unreacted salts. The synthesized nanoparticles were black in color and were subsequently dried overnight at 150°C. This process ensured the production of famatinite nanoparticles with the desired properties for further characterization.

#### 2.3. Characterization

The synthesized Cu $_3$ SbS $_4$  nanoparticles were characterized by Powder X-ray diffraction (BRUKER-binary V4) equipped with Cu-K alpha1 ( $\lambda$ =1.54060 Å, 40 kV, 30 mA and step width 0.04). The phase of the synthesized nanoparticles was confirmed by Raman analysis technique (Invia reflex raman microscope with spectrometer) with an excitation of 785 nm near IR laser light. The morphology, particle size and chemical composition were determined by Scanning electron microscopy and Energy dispersive spectrometer (SEM with EDS, ZEISS at accelerating voltage of 10 KV). The optical properties of the nanoparticles were determined by UV Diffuse reflectance spectroscopy, (SHIMADZU UV 2600) in the range of 220 – 1400 nm.

#### 3. Results and discussion

#### 3.1. Structural analysis

The structure, crystallite size and phase of the synthesized nanoparticles with different PVP ratios of PVP0, PVP0.5, PVP1.0 and PVP1.5 were analysed using XRD technique. Fig. 1 represents the XRD patterns of all the above samples and their comparison with JCPDS (PDF: 01–085–1344) card. The XRD patterns of all these samples confirmed the famatinite ( $Cu_3SbS_4$ ) phase of nanoparticles and they have tetragonal crystal structure.

PVP<sub>0</sub> displays the famatinite (Cu<sub>3</sub>SbS<sub>4</sub>) phase at specific angles  $2\theta = 28.81^\circ$ , 29.98, 33.28, 47.88 and 56.75, corresponding to planes (112), (103), (200), (204) and (312) respectively [36]. Additionally, it shows the presence of chalcostibite (CuSbS<sub>2</sub>) phase at  $2\theta = 49.88^\circ$ , identified with the (521) plane [32]. Meanwhile, PVP<sub>1.5</sub> reveals the famatinite phase at  $2\theta = 28.67$ , 29.89, 33.13, 47.92 and 56.57, associated with planes (112), (103), (200), (204) and (312) [36] along with chalcostibite peaks at  $2\theta = 49.81^\circ$  and 54.28, linked to planes (521) and (621) respectively (PDF: 00-044-1417) [32]. However, both PVP<sub>0.5</sub> and PVP<sub>1.0</sub> exclusively exhibit the famatinite phase at  $2\theta = 28.69^\circ$ , 29.85,

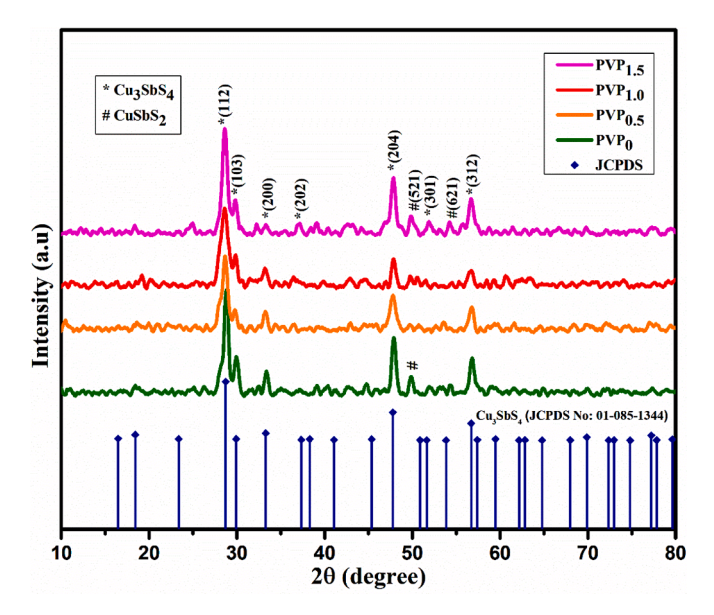


Fig. 1. XRD pattern of  $Cu_3SbS_4$  nanoparticles prepared with different PVP ratios.

33.20°, 47.75° and 56.69°, corresponding to planes (112), (103), (200), (204) and (312), and at  $2\theta=28.61^\circ$ , 29.90°, 33.30°, 47.73°, and 56.62°, attributed to planes (112), (103), (200), (204), and (312) respectively. Shigeru Ikeda et al. synthesized Cu<sub>3</sub>SbS<sub>4</sub> nanoparticles which shows sharp peaks in XRD analysis at angles  $2\theta=28.5^\circ$ , 32.5°, 47.5° and 56.5° attributed to planes (112), (200), (204) and (312) respectively (30). These findings align well with the values in the JCPDS card (PDF: 01–085–1344) for Cu<sub>3</sub>SbS<sub>4</sub> nanoparticles and (PDF: 00–044–1417) for CuSbS<sub>2</sub> nanoparticles.

The crystallite size of the nanoparticles was calculated using Debye Scherrer's formula

$$D = \frac{K\lambda}{(\beta cos\theta)}$$

Where K – Scherrer's constant (K = 0.89)

 $\lambda$  – wavelength of the radiation used Cu-K alpha 1 ( $\lambda$ = 1.54060 Å)

 $\beta$  – full width at half maximum of the diffraction peaks

 $\theta$  – bragg's angle

Table 1 demonstrates the average crystallite sizes of the synthesized  $\text{Cu}_3\text{SbS}_4$  nanoparticles (PVP0, PVP0.5, PVP1.6, PVP1.5). The addition of PVP played a crucial role in diminishing the crystallite size of the nanoparticles. As seen in Table 1, PVP0.5 demonstrates a smaller crystallite size of 20.405 nm, while PVP0 displays a larger crystallite size of 30.664 nm. Meanwhile, PVP1.0 and PVP1.5 exhibit crystallite sizes of 23.916 nm and 25.183 nm respectively. Incrementally adding more PVP, in 0.5 g steps, results in an expansion of the crystallite size. Nevertheless, these crystallite sizes consistently remain smaller than those observed in nanoparticles prepared without PVP, i.e., PVP0.

Theoretical values of lattice parameters from JCPDS card (PDF: 01-085-1344) and observed values are also listed in table 1. It is observed that the lattice parameter values of the four synthesised nanoparticles (PVP<sub>0</sub>, PVP<sub>0.5</sub>, PVP<sub>1.0</sub>, and PVP<sub>1.5</sub>) nearly match with the values found in the JCPDS dataset (PDF: 01-085-1344) as well as in the reported values. Erika Dutkova et al. synthesized Cu<sub>3</sub>SbS<sub>4</sub> nano powders with lattice parameters a=b=5.3911 Å and c=10.7633 Å[37]. However, compared to the other nanoparticles, the lattice parameter values of PVP<sub>0.5</sub> has more consistency with JCPDS readings. Table 2

Raman analysis has been carried out to all the four samples (PVP $_0$ , PVP $_0$ .5, PVP $_1$ .0 and PVP $_1$ .5) in order to confirm the phases present in the process of synthesizing phase pure Cu $_3$ SbS $_4$ . The spectrum ranging from 200 cm $^{-1}$  to 800 cm $^{-1}$  is depicted in the graph in Fig. 2. This analysis utilized near-infrared laser light, specifically at 785 nm for excitation. The Raman spectrum (Fig. 2) indicates that all four samples exhibit a mode at 314 cm $^{-1}$ , corresponding to the Cu $_3$ SbS $_4$  phase which is further validated by RRUFF data (RRUFF ID: R110022). The spectrum seen in PVP $_0$  and PVP $_1$ .5 revealed an additional mode at 328 cm $^{-1}$ , corresponding to the CuSbS $_2$  phase, signifying the presence of this secondary phase in these two samples. This observation is supported by RRUFF data (RRUFF ID: R060262). The identified findings unveiled that PVP $_0$ 5 and PVP $_1$ 0 exhibited phase-pure famatinite nanoparticles, aligning well with the outcomes derived from XRD analysis.

#### 3.2. Morphological and compositional analysis

The morphology and compositional analysis of the synthesized nanoparticles (PVP $_0$ , PVP $_{0.5}$ , PVP $_{1.0}$  and PVP $_{1.5}$ ) are investigated using Scanning electron microscopy with Energy dispersive spectroscopy. Fig. 3. (a–d) represents the SEM images of the synthesized nanoparticles with different PVP ratios. In Fig. 3(a), the morphology of PVP $_0$  is depicted, featuring nanoparticles displaying a spherical shape. Notably, this image emphasizes the agglomeration of the nanoparticles, indicating the absence of PVP during synthesis. Fig. 3(b) presents the morphology of PVP $_{0.5}$ , showcasing nanoparticles with a clearly defined spherical structure. This image highlights the absence of agglomeration,

 $\begin{tabular}{ll} \textbf{Table 2} \\ \textbf{Compositional analysis of the synthesized $Cu_3SbS_4$ nanoparticles with different PVP ratios.} \end{tabular}$ 

Sample	Element/Series	Weight%	Atomic%	{[Cu]+[Sb]}/[S]	
PVP <sub>0</sub>	Cu L	25	38	1.43	
	Sb L	25	21		
	S K	50	41		
$PVP_{0.5}$	Cu L	30	42	1.36	
	Sb L	42	15		
	S K	28	42		
$PVP_{1.0}$	Cu L	27	37	1.41	
	Sb L	22	21		
	S K	51	41		
$PVP_{1.5}$	Cu L	21	32	1.13	
	Sb L	27	21		
	S K	52	47		

 $\label{thm:continuous} \textbf{Table 1} \\ \textbf{The average crystallite size and observed lattice values of $Cu_3SbS_4$ nanoparticles synthesized with different PVP ratios.} \\$ 

Name of the sample	Average crystallite size (D) nm	Lattice val	Lattice values - Observed			Lattice values - JCPDS (PDF: 01-085-1344)		
		a(Å)	b(Å)	c(Å)	a(Å)	b(Å)	c(Å)	
PVP <sub>0</sub> (180°C)	30.664	5.379	5.379	10.659	5.380	5.380	10.760	
PVP <sub>0.5</sub> (180°C)	20.405	5.392	5.392	10.740	5.380	5.380	10.760	
PVP <sub>1.0</sub> (180°C)	23.916	5.376	5.376	10.885	5.380	5.380	10.760	
PVP <sub>1.5</sub> (180°C)	25.183	5.402	5.402	10.715	5.380	5.380	10.760	

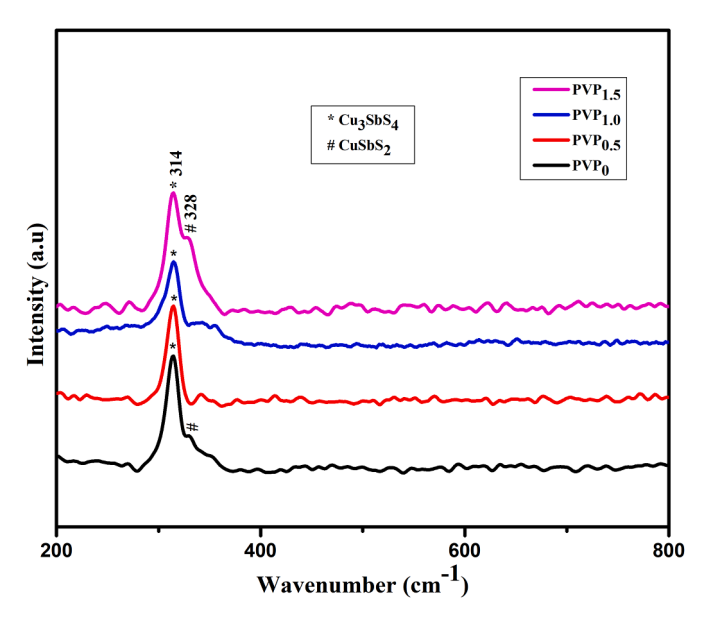


Fig. 2. Raman spectra of Cu<sub>3</sub>SbS<sub>4</sub> nanoparticles synthesized with different PVP ratios.

a result of the incorporation of 0.5 g of PVP during synthesis. Fig. 3(c) displays the spherical morphology of PVP<sub>1.0</sub>, revealing a lesser degree of agglomeration compared to PVP<sub>0</sub>. In Fig. 3(d), the morphology of PVP<sub>1.5</sub> is shown, exhibiting a spherical structure with reduced agglomeration compared to PVP<sub>1.0</sub>. Evidently, increasing the amount of PVP in the synthesis process diminishes agglomeration and leads to a reduction in the size of the spherical particles. Among these, nanoparticles synthesized with 0.5 g of PVP (PVP<sub>0.5</sub>) demonstrate the most desirable characteristics: a well-defined spherical morphology without any agglomeration. Similar morphology was observed in the Cu<sub>3</sub>SbS<sub>4</sub>

nanoparticles synthesized by Bella et al. via surfactant assisted solvothermal synthesis [11].

Fig. 4 (a-d) represents the EDX patterns of the synthesized  $\text{Cu}_3\text{SbS}_4$  nanoparticles with different PVP ratios (PVP0, PVP0.5, PVP1.0 and PVP1.5). The quantities of sulphur, antimony, and copper in the synthesised nanoparticles are determined by analysing their elemental composition using the Cu L, Sb L, and S K series in EDX analysis. The Cu: Sb:S ratios of the synthesized nanoparticles PVP0.5 almost corresponds to  $\text{Cu}_3\text{SbS}_4$  whereas, for PVP1.5 the ratio is close to 1. Fig. 5 depicts the elemental mapping of Cu, Sb, S nanoparticles of PVP0.5. From the images it can be concluded that the dispersion of the resulting  $\text{Cu}_3\text{SbS}_4$  nanoparticles is homogenous and uniform.

#### 3.3. Optical properties of Cu<sub>3</sub>SbS<sub>4</sub> nanoparticles

Fig. 6 (a & b) represents the optical absorption and reflectance spectrum of the synthesized Cu<sub>3</sub>SbS<sub>4</sub> nanoparticles (PVP<sub>0</sub>, PVP<sub>0.5</sub>,  $PVP_{1.0}$  and  $PVP_{1.5}$ ). In the absorption spectrum it is seen that  $PVP_{0.5}$  and PVP<sub>1.0</sub> shows continuous absorption in the entire visible region and the near IR region. Both samples exhibit a drop in absorption around 1350 nm [23,38], which corresponds to the reported absorption edge of Cu<sub>3</sub>SbS<sub>4</sub> nanoparticles. A dip in the curve near 800 nm [39,40] corresponds to the CuSbS2 phase observed in PVP0 and PVP1.5. Bincy John et al. performed UV - Diffused Reflectance Spectroscopy for their synthesized nanoparticles with absorption over entire visible region and the absorption sharply descended around 800 nm indicating CuSbS2 phase (37). The additional phase of CuSbS2 is confirmed in XRD and Raman analysis. Following the decline at 800 nm, there's a consistent absorption observed up to 1350 nm in both PVP<sub>0</sub> and PVP<sub>1.5</sub> corresponding to Cu<sub>3</sub>SbS<sub>4</sub> phase. From Fig. 6(b) it is clear that the diffuse reflectance of PVP<sub>0</sub> and PVP<sub>1.5</sub> descends around 800 nm to the lower wavelength region which corresponds to CuSbS2 phase. The absorption of all the four samples covered entire visible region and for PVP<sub>0.5</sub> and PVP<sub>1.0</sub> it is upto near IR region. This is very ideal for materials intended for photovoltaic application since the absorbance coverd the entire visible region as well

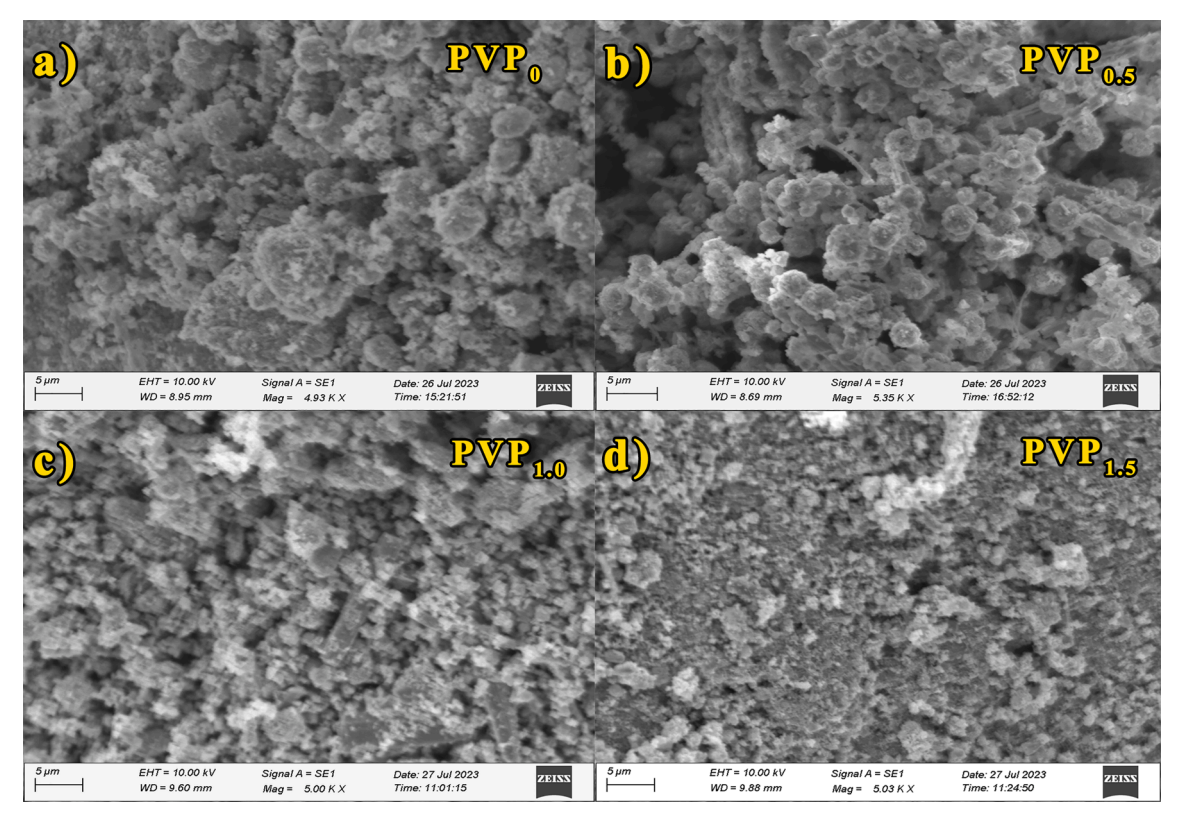


Fig. 3. SEM images of the synthesized Cu<sub>3</sub>SbS<sub>4</sub> nanoparticles with different PVP ratios (a)PVP<sub>0</sub>, (b) PVP<sub>0.5</sub>, (c) PVP<sub>1.0</sub>, (d)PVP<sub>1.5</sub>.

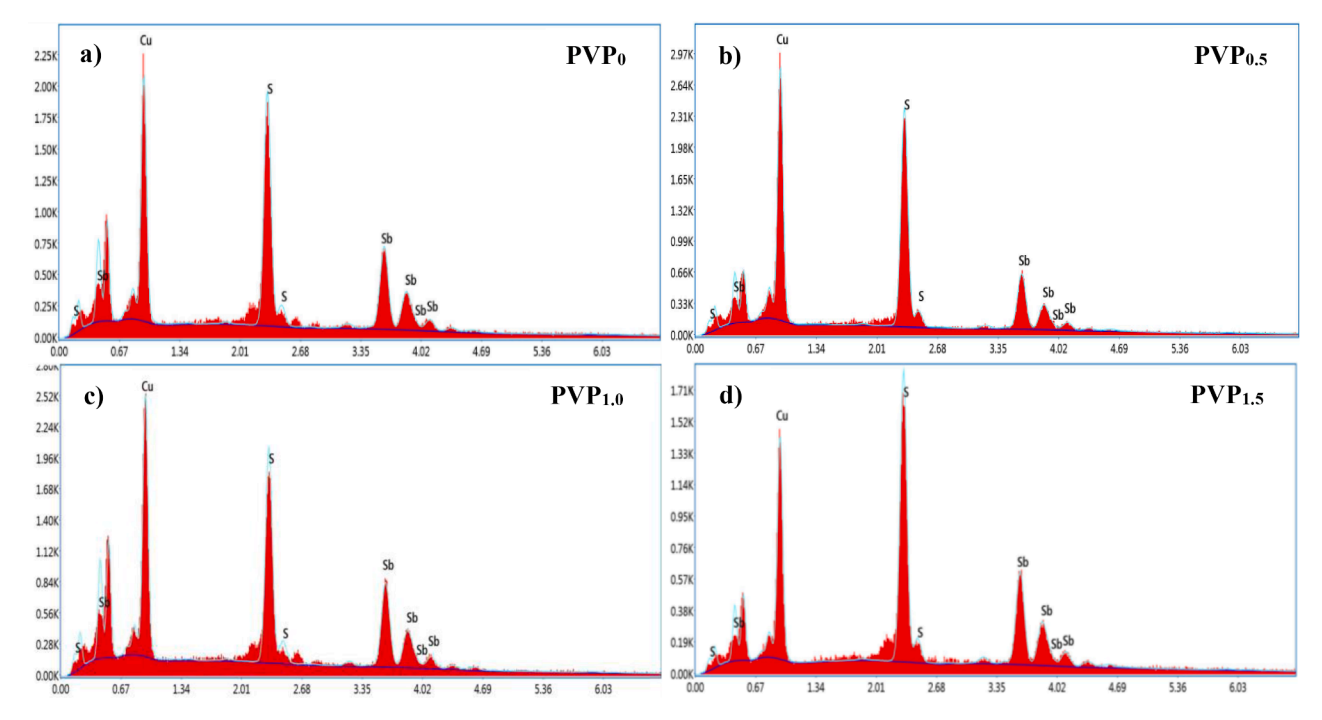


Fig. 4. EDX patterns of the synthesized Cu<sub>3</sub>SbS<sub>4</sub> nanoparticles with different PVP ratios (a) PVP<sub>0</sub>, (b) PVP<sub>0.5</sub>, (c)PVP<sub>1.0</sub>, (d)PVP<sub>1.5</sub>.

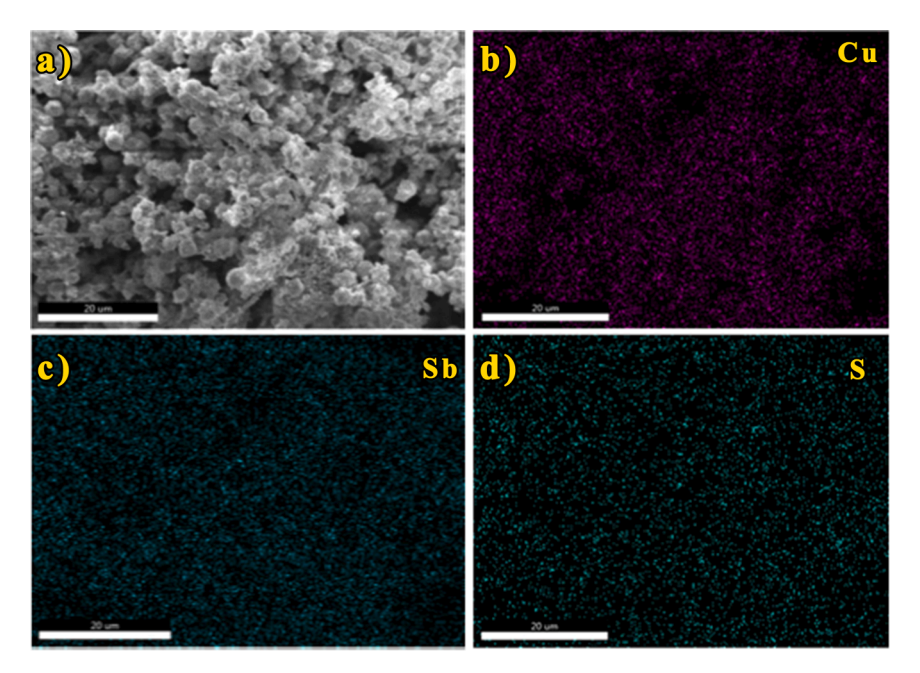


Fig. 5. (a) SEM image and (b), (c), (d) the elemental mapping of Cu, Sb and S of synthesized Cu<sub>3</sub>SbS<sub>4</sub> nanoparticles (PVP<sub>0.5</sub>).

as the near infrared region.

Optical bandgap values of the samples were determined using Kubelka-Munk transformations. The relation for Kubelka-Munk transformations is

$$F(R) = \frac{\left(1 - R\right)^2}{2R}$$

Where,

F(R) - Kubelka-Munk function

R - Reflectance (%)

Fig. 6(c) represents the bandgap diagram of the synthesized  $\text{Cu}_3\text{SbS}_4$  nanoparticles with different PVP ratios (PVP<sub>0</sub>, PVP<sub>0.5</sub>, PVP<sub>1.0</sub> and

PVP<sub>1.5</sub>). The direct bandgap energies of the synthesized nanoparticles were determined by extrapolating the linear portion of the graph correlating the modified Kubelka-Munk function  $(F(R)h\nu)^2$  and photon energy  $(h\nu)$ , where h represents Planck's constant and  $\nu$  stands for frequency. The synthesised Cu<sub>3</sub>SbS<sub>4</sub> nanoparticles PVP<sub>0</sub>, PVP<sub>0.5</sub>, PVP<sub>1.0</sub> and PVP<sub>1.5</sub> possess the estimated bandgap energies of 0.97 eV, 0.88 eV, 0.92 eV and 0.94 eV respectively. This is the ideal value for a material intended for photovoltaic absorber layer and the above results were perfectly matched with the reported values. G. H. Albuquerque et al. reported a bandgap value of 0.9 eV for Cu<sub>3</sub>SbS<sub>4</sub> films for the application of solar cell absorber material [41]. Qiang Zeng et al. conducted UV–Vis spectrophotometry on the Cu<sub>3</sub>SbS<sub>4</sub> nanocrystals they synthesized,

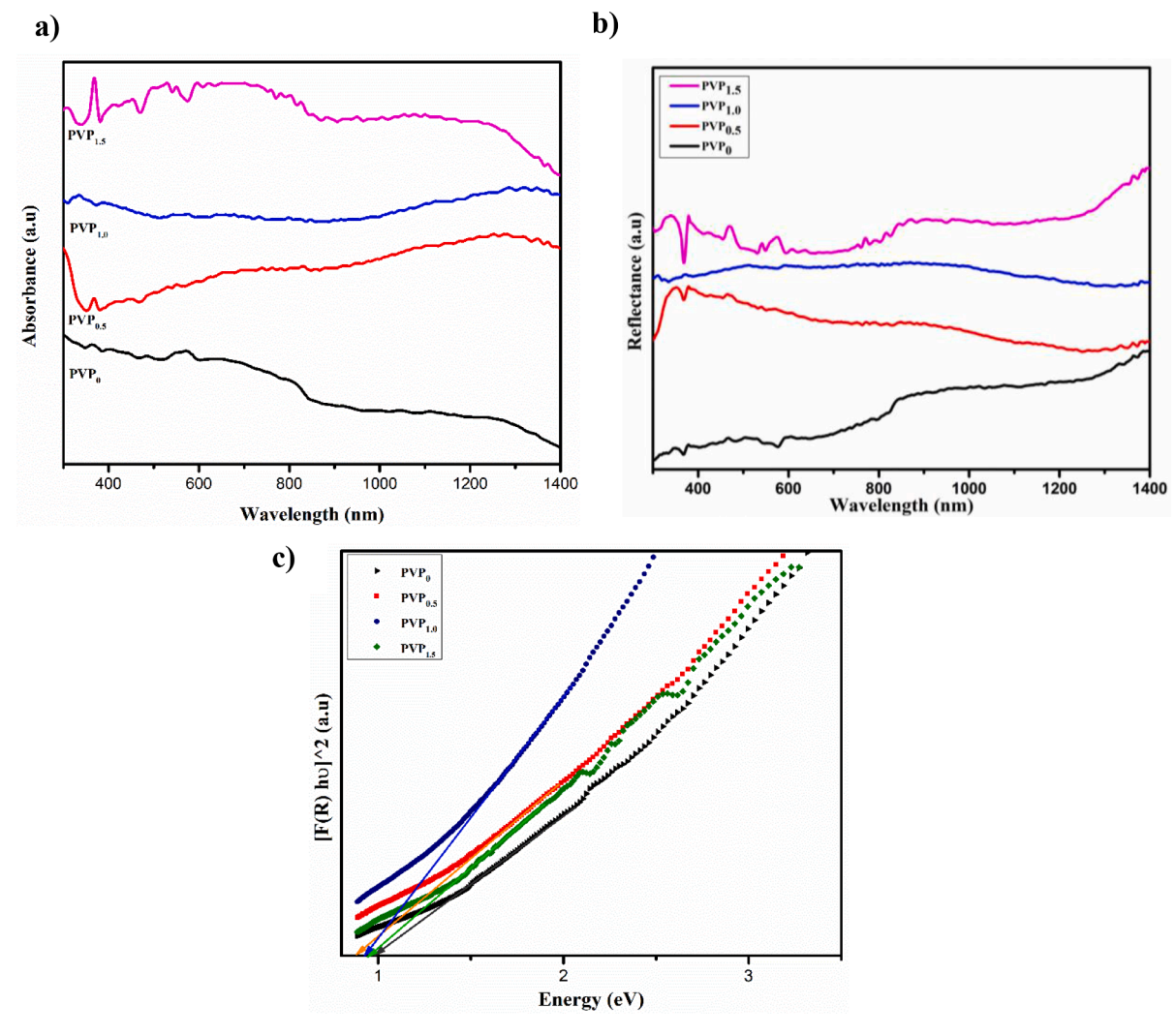


Fig. 6. a) Absorption spectra and b) Reflectance spectra and c) Band gap calculation of synthesized Cu<sub>3</sub>SbS<sub>4</sub> nanoparticles with different PVP ratios.

revealing a strong absorption edge at approximately below 1300 nm. They further determined the optical band gap of the  $\text{Cu}_3\text{SbS}_4$  nanocrystals as 0.89 eV [38]. It is clearly seen that PVP plays a major role in defining the bandgap values of the synthesized  $\text{Cu}_3\text{SbS}_4$  nanoparticles. The  $\text{Cu}_3\text{SbS}_4$  nanoparticles synthesized with 0.5 g PVP (PVP $_{0.5}$ ) exhibits the optimum bandgap value of 0.88 eV for photovoltaic application.

# 4. Conclusion

Cu<sub>3</sub>SbS<sub>4</sub> nanoparticles were synthesized using different ratios of polyvinylpyrrolidone (PVP) via a solvothermal method employing a binary solvent. All four samples exhibited the famatinite phase and tetragonal crystal structure, matching the data from the JCPDS card.  $PVP_{0.5}$  and  $PVP_{1.0}$  demonstrated a phase-pure famatinite phase, whereas PVP<sub>0</sub> and PVP<sub>1.5</sub> exhibited an additional chalcostibite phase. The crystallite size of the nanoparticles ranged from 20.405 nm to 30.664 nm, with PVP<sub>0.5</sub> exhibiting the smallest crystallite size of 20.405 nm. Raman analysis highlighted the significant influence of PVP on phase formation, resulting in the production of phase-pure Cu<sub>3</sub>SbS<sub>4</sub> with PVP<sub>0.5</sub> and PVP<sub>1.0</sub>, while PVP<sub>0</sub> and PVP<sub>1.5</sub> exhibited an additional CuSbS<sub>2</sub> phase. These results were consistent with RRUFF data. Despite all four samples having a sphere-like morphology, PVP<sub>0.5</sub> showed less agglomeration compared to the others. Optical studies indicated absorption across the entire visible and near-infrared regions for all samples and absorption edge falling around 1350 nm, confirming the Cu<sub>3</sub>SbS<sub>4</sub> phase. However,

 $PVP_0$  and  $PVP_{1.5}$  exhibited a drop around 800 nm, indicating the presence of the  $CuSbS_2$  phase. The estimated bandgap values for  $PVP_0, \, PVP_{0.5}, \, PVP_{1.0}, \, and \, PVP_{1.5}$  were 0.97 eV, 0.88 eV, 0.92 eV, and 0.94 eV, respectively. These comprehensive findings suggest  $Cu_3SbS_4$  as a promising candidate for a photovoltaic absorber material in the photovoltaic sector.

#### CRediT authorship contribution statement

**Prakash Iruthayanathan:** Writing – original draft, Validation, Methodology, Investigation, Data curation. **Anne Sarah Christinal:** Visualization, Formal analysis. **Amutha Soosairaj:** Writing – review & editing, Resources. **Leo Rajesh Asirvatham:** Validation, Supervision, Resources, Conceptualization.

#### **Declaration of competing interest**

The authors declare that they have no known competing financial interests or personal relationships that could have appeared to influence the work reported in this paper.

# Data availability

The data are included in the manuscript in the form of figures and tables.

#### References

- E. Peccerillo, K. Durose, Copper—Antimony and copper—Bismuth chalcogenides—Research opportunities and review for solar photovoltaics, MRS Energy Sustain 5 (1) (2018) 1–59, https://doi.org/10.1557/mre.2018.10.
- [2] A. Soosairaj, D.P. Pabba, A. Gunasekaran, S. Anandan, Synergetic impact of natural light harvesting materials to reduce the recombination rate and improve the device performance of dye sensitized solar cells, J. Mater. Sci. Mater. Electron. (2023) 1–13, https://doi.org/10.1007/s10854-023-11172-5.
- [3] L. Rajesh, Deposition and characterization of spray pyrolysed p-type Cu2SnS3 thin film for potential absorber layer of solar cell, Phys. B Phys. Condens. Matter (2018), https://doi.org/10.1016/j.physb.2018.03.007.
- [4] B. Yang, et al., CuSbS2 as a promising earth-abundant photovoltaic absorber material: a combined theoretical and experimental study, Chem. Mater. 26 (10) (2014) 3135–3143, https://doi.org/10.1021/cm500516v. May.
- [5] M.A. Green, Y. Hishikawa, E.D. Dunlop, D.H. Levi, J. Hohl-Ebinger, A.W.Y. Ho-Baillie, Solar cell efficiency tables (version 51, Prog. Photovoltaics Res. Appl. 26 (1) (2018) 3–12, https://doi.org/10.1002/pip.2978.
- [6] A. Soosairaj, A. Gunasekaran, S. Anandan, L. Rajesh, Synergetic effect of Leucophyllum frutescens and Ehretia microphylla dyes in enhancing the photovoltaic performance of dye - sensitized solar cells, Environ. Sci. Pollut. Res. (2023) 52895–52905, https://doi.org/10.1007/s11356-023-26132-z.
- [7] C. Yan, et al., Cu2ZnSnS4 solar cells with over 10% power conversion efficiency enabled by heterojunction heat treatment, Nat. Energy 3 (9) (2018) 764–772, https://doi.org/10.1038/s41560-018-0206-0.
- [8] M. Liu, M.B. Johnston, H.J. Snaith, Efficient planar heterojunction perovskite solar cells by vapour deposition, Nature 501 (7467) (2013) 395–398, https://doi.org/ 10.1038/nature12509
- [9] R. Suriakarthick, V. Nirmal Kumar, T.S. Shyju, R. Gopalakrishnan, Effect of substrate temperature on copper antimony sulphide thin films from thermal evaporation, J. Alloys Compd. 651 (2015) 423–433, https://doi.org/10.1016/j. iallcom.2015.08.061. Dec.
- [10] S. Thiruvenkadam and A.L. Rajesh, "Effect Of Antimony concentration on the properties of spray pyrolysed Cusbs 2 thin film absorbing layer for photovoltaic application," vol. 3, no. 2, pp. 2–5, 2014.
- [11] M. Bella, C. Rivero, S. Blayac, H. Basti, M.C. Record, P. Boulet, Oleylamine-assisted solvothermal synthesis of copper antimony sulfide nanocrystals: morphology and phase control, Mater. Res. Bull. 90 (2017) 188–194, https://doi.org/10.1016/j. materresbull.2017.02.036. Jun.
- [12] L. Shi, C. Wu, J. Li, J. Ding, Selective synthesis and photoelectric properties of Cu3SbS4and CuSbS2 nanocrystals, J. Alloys Compd. 694 (2017) 132–135, https://doi.org/10.1016/j.jallcom.2016.09.307.
- [13] E. Dutková, et al., Nanocrystalline Skinnerite (Cu3SbS3) prepared by high-energy milling in a laboratory and an industrial mill and its optical and optoelectrical properties, Molecules 28 (1) (2023), https://doi.org/10.3390/ molecules28010326.
- [14] C. Tablero, Electronic and optical property analysis of the Cu-Sb-S tetrahedrites for high-efficiency absorption devices, J. Phys. Chem. C 118 (28) (2014) 15122–15127, https://doi.org/10.1021/jp502045w.
- [15] M. Yıldırım, A. Aljabour, A. Sarılmaz, F. Özel, Investigation of optical framework of chalcostibite nanocrystal thin films: an insight into refractive index dispersion, optical band gap and single-oscillator parameters, J. Alloys Compd. 722 (2017) 420–426, https://doi.org/10.1016/j.jallcom.2017.06.157.
- [16] K. Ramasamy, H. Sims, W.H. Butler, A. Gupta, Selective nanocrystal synthesis and calculated electronic structure of all four phases of copper-antimony-sulfide, Chem. Mater. 26 (9) (2014) 2891–2899, https://doi.org/10.1021/cm5005642. May.
- [17] C. Behera, R. Samal, C.S. Rout, R.S. Dhaka, G. Sahoo, S.L. Samal, Synthesis of CuSbS2 nanoplates and CuSbS2-Cu3SbS4 nanocomposite: effect of sulfur source on different phase formation, Inorg. Chem. 58 (22) (2019) 15291–15302, https://doi. org/10.1021/acs.inorgchem.9b02291.
- [18] U. Chalapathi, B. Poornaprakash, S.H. Park, Growth and properties of Cu3SbS4 thin films prepared by a two-stage process for solar cell applications, Ceram. Int. 43 (6) (2017) 5229–5235, https://doi.org/10.1016/j.ceramint.2017.01.048. Apr.
- [19] B. Du, R. Zhang, M. Liu, K. Chen, H. Zhang, M.J. Reece, Crystal structure and improved thermoelectric performance of iron stabilized cubic Cu3SbS3 compound, J. Mater. Chem. C 7 (2) (2019) 394–404, https://doi.org/10.1039/c8tc05301d.
- [20] G. Chen, et al., Study on the synthesis and formation mechanism of flower-like Cu3SbS4 particles via microwave irradiation, J. Alloys Compd. 679 (2016) 218–224, https://doi.org/10.1016/j.jallcom.2016.04.042. Sep.
- [21] C. An, Y. Jin, K. Tang, Y. Qian, Selective synthesis and characterization of famatinite nanofibers and tetrahedrite nanoflakes, J. Mater. Chem. 13 (2) (2003) 301–303, https://doi.org/10.1039/b210703a. Feb.

- [22] S. Kaowphong, N. Chumha, Solvothermal synthesis of CuInS2 nanoparticles in ethylene glycol-water medium and their photovoltaic properties, Russ. J. Inorg. Chem. 64 (11) (2019) 1469–1474, https://doi.org/10.1134/S003602361911007X. Nov
- [23] J. Van Embden, Y. Tachibana, Synthesis and characterisation of famatinite copper antimony sulfide nanocrystals, J. Mater. Chem. 22 (23) (2012) 11466–11469, https://doi.org/10.1039/c2jm32094k. Jun.
- [24] R.B. Balow, C.K. Miskin, M.M. Abu-Omar, R. Agrawal, Synthesis and characterization of Cu3(Sb1-xAsx)S4 semiconducting nanocrystal alloys with tunable properties for optoelectronic device applications, Chem. Mater. 29 (2) (2017) 573–578, https://doi.org/10.1021/acs.chemmater.6b03850. Jan.
- [25] Q. Wang, J. Li, J. Li, Enhanced thermoelectric performance of Cu3SbS4 flower-like hierarchical architectures composed of Cl doped nanoflakes via an in situ generated CuS template, Phys. Chem. Chem. Phys. 20 (3) (2018) 1460–1475, https://doi.org/10.1039/c7cp06465a.
- [26] M. Pal, Y. Torres Luna, R. Silva González, N.R. Mathews, F. Paraguay-Delgado, U. Pal, Phase controlled synthesis of CuSbS2 nanostructures: effect of reaction conditions on phase purity and morphology, Mater. Des. 136 (2017) 165–173, https://doi.org/10.1016/j.matdes.2017.09.059.
- [27] A.H. Alshammari, K. Alshammari, M. Alshammari, T.A.M. Taha, Structural and optical characterization of g-C3N4 nanosheet integrated PVC/PVP polymer nanocomposites, Polymers (Basel) 15 (4) (2023), https://doi.org/10.3390/polym15040871.
- [28] A.H. Alshammari, T.A. Taha, Structure, thermal and dielectric insights of PVC/PVP/ZnFe2O4 polymer nanocomposites, Eur. Phys. J. Plus 136 (12) (2021), https://doi.org/10.1140/epip/s13360-021-02206-0.
- [29] A.H. Alshammari, M. Alshammari, M. Ibrahim, K. Alshammari, T.A.M. Taha, New Hybrid PVC/PVP polymer blend modified with Er2O3 nanoparticles for optoelectronic applications, Polymers 15 (3) (2023) 1–13, https://doi.org/ 10.3390/polym15030684.
- [30] V. Bhavsar, D. Tripathi, Structural, optical, and aging studies of biocompatible PVC-PVP blend films, J. Polym. Eng. 38 (5) (2018) 419–426, https://doi.org/ 10.1515/polyeng-2017-0184.
- [31] A.H. Alshammari, M. Alshammari, K. Alshammari, N.K. Allam, T.A. Taha, PVC/ PVP/SrTiO3 polymer blend nanocomposites as potential materials for optoelectronic applications, Results Phys. 44 (December 2022) (2023) 106173, https://doi.org/10.1016/j.rinp.2022.106173.
- [32] J. Bincy, S.G. G, R.A. L, Temperature dependent solvothermal synthesis of Cu-Sb-S nanoparticles with tunable structural and optical properties, Mater. Res. Bull. 95 (2017) 267–276, https://doi.org/10.1016/j.materresbull.2017.07.026.
- [33] K.M. Koczkur, S. Mourdikoudis, L. Polavarapu, S.E. Skrabalak, Polyvinylpyrrolidone (PVP) in nanoparticle synthesis, Dalt. Trans. 44 (41) (2015) 17883–17905, https://doi.org/10.1039/c5dt02964c.
- [34] B. John, G. Genifer Silvena, S. Hussain, M.C. Santhosh Kumar, A. Leo Rajesh, Surfactant-mediated solvothermal synthesis of CuSbS 2 nanoparticles as p-type absorber material, Indian J. Phys. 93 (2) (2019) 185–195, https://doi.org/ 10.1007/s12648-018-1288-z.
- [35] W. Wang, et al., Effect of PVP content on photocatalytic properties of CuSbS2 particles with chemical etching, J. Nanoparticle Res. 22 (9) (2020), https://doi.org/10.1007/s11051-020-05024-0.
- [36] S. Ikeda, S. Sogawa, Y. Tokai, W. Septina, T. Harada, M. Matsumura, Selective production of CuSbS2, Cu3SbS3, and Cu3SbS4nanoparticles using a hot injection protocol, RSC Adv. 4 (77) (2014) 40969–40972, https://doi.org/10.1039/ c4ra07648f.
- [37] E. Dutková, M. Jesús Sayagués, M. Fabián, M. Baláž, M. Achimovičová, Mechanochemically synthesized ternary chalcogenide Cu3SbS4 powders in a laboratory and an industrial mill, Mater. Lett. 291 (2021) 3–7, https://doi.org/ 10.1016/i.matlet.2021.129566.
- [38] Q. Zeng, et al., Famatinite Cu3SbS4 nanocrystals as hole transporting material for efficient perovskite solar cells, J. Mater. Chem. C 6 (30) (2018) 7989–7993, https://doi.org/10.1039/C8TC02133C.
- [39] B. John, G.Genifer Silvena, A. Leo Rajesh, Influence of reaction time on the structural, optical and electrical performance of copper antimony sulfide nanoparticles using solvothermal method, Phys. B Condens. Matter. 537 (2018) 243–250, https://doi.org/10.1016/j.physb.2018.02.030.
- [40] L. Shi, Y. Li, C. Wu, Y. Dai, Preparation, formation mechanism and photoelectric properties of well-aligned CuSbS 2 nanowires, J. Alloys Compd. 648 (2015) 507–511, https://doi.org/10.1016/j.jallcom.2015.07.030.
- [41] G.H. Albuquerque, et al., Multimodal characterization of solution-processed Cu3SbS4 absorbers for thin film solar cells, J. Mater. Chem. A 6 (18) (2018) 8682–8692, https://doi.org/10.1039/C8TA00001H.